Appendix
Imperfections Measuring System

A.1 Introduction

The Imperfections Measuring System (IMS) or "*shapemeter*" is based on publications by Arbocz and co-workers [1–3] and we developed it to validate our finite element models comparing numerical with experimental results [4]. The IMS was used to survey the geometry of the pipes that were tested in collapse facilities at Tenaris Siderca (Argentina) and at C-FER Technologies (Canada). A photograph of the IMS is shown in Fig. A.1.

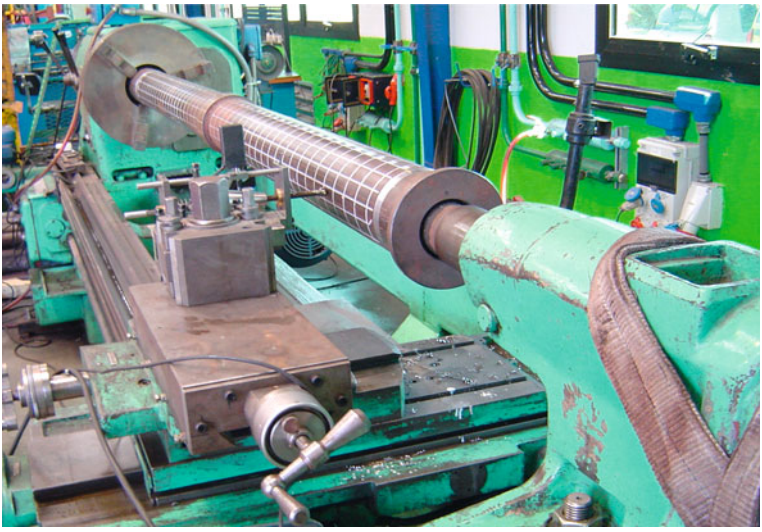

Fig. A.1 The IMS (or shapemeter)

E. N. Dvorkin and R. G. Toscano, *Finite Element Analysis of the Collapse and Post-Collapse Behavior of Steel Pipes: Applications to the Oil Industry*, SpringerBriefs in Computational Mechanics, DOI: 10.1007/978-3-642-37361-9,

A.2 Mapping of the Sample External Surfaces

The samples are rotated in the lathe and on its carriage an linear variable displacement transducer (LVDT) is placed. The LVDT touches the external surface of the rotating samples and at regular intervals of time its radial position is recorded; also, the angular position of the samples is recorded at the same time intervals by a rotary encoder.

We developed an algorithm to obtain from the acquired data a Fourier series description of the external surface of the samples [4].

A.2.1 Algorithm to Process the Data Acquired with the IMS

The data are acquired along a spiral path; however, in subsequent analyses we will consider that the points corresponding to a turn are located on a planar section, at an axial distance z_k from an arbitrary origin. As the pitch of the spiral is less than half of the typical wall thickness under analysis, this assumption is valid for the purpose of modeling the collapse tests.

The data are fitted to a perfect circle (of unknown center and radius) through a least squares method [3]. This approach is consistent with the subsequent Fourier decomposition (see Fig. A.2).

Input data

r_j radial distance from the rotation axis to the external surface, jth data point.

q_j total turns corresponding to the jth data point, measured from an arbitrary defined zero.

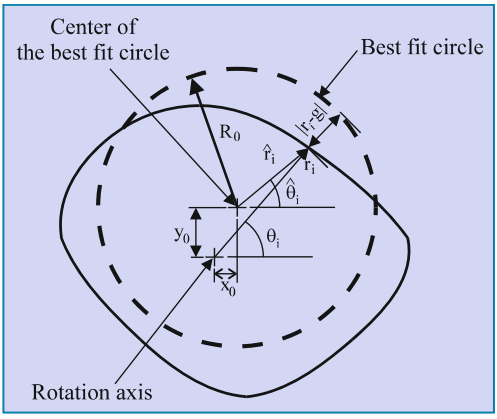

Fig. A.2 Algorithm to process the data acquired with the LVDT

Algorithm

Initial data reduction

We can define $k = int(q_j)$ the *kth* turn. For this turn we have,

$$\begin{aligned} z_k &= \Delta z \cdot \mathrm{int}(q_j) \\ \theta_i^k &= 2\pi\big(q_j - \mathrm{int}(q_j)\big) \\ r_i^k &= r_j \end{aligned}$$

where $i = 1$ for the first j which satisfies $(\mathrm{q} - \mathrm{int}(\mathrm{q_j})) > 0$ (indication of a new turn). Δz indicates the axial advance per turn. The number of data points per turn is not constant.

Fit to best circle

For the kth section we can define a "best-fit circle", with radius $\mathrm{R_0}$ and with its center located at ($\mathrm{x_0}$, $\mathrm{y_0}$) in a Cartesian system, contained in the section plane and with its origin at the section rotation center [3]. The superindex k in $\theta_\mathrm{i}^\mathrm{k}$ and $\mathrm{r_i^k}$ is omitted.

For determining $\mathrm{R_0}$, $\mathrm{x_0}$ and $\mathrm{y_0}$ we solve the following minimization problem,

$$\begin{aligned} (R_0, x_0, y_0) &= \arg[\min E_2(R_0, x_0, y_0)] \\ E_2 &= \sum_i [r_i - g(\theta_i, R_0, x_0, y_0)]^2 \\ g(\theta_i, R_0, x_0, y_0) &= (x_0 \cos\theta_i + y_0 \sin\theta_i) + \sqrt{R_0^2 - (x_0 \sin\theta_i - y_0 \cos\theta_i)^2} \end{aligned}$$

To solve the above nonlinear minimization problem we apply the Levemberg-Marquard method [5], using as first trial a simplified (linearized) solution in which the expression for g reduces to [6],

$$g_{lin}(\theta_i, R_0, x_0, y_0) = (x_0 \cos\theta_i + y_0 \sin\theta_i) + R_0$$

Data reduction to new center

Once the center of the "best-fit circle" is determined we reduce the acquired data to it,

$$\begin{aligned} \hat{x}_i &= r_i \cos\theta_i - x_0 \\ \hat{y}_i &= r_i \sin\theta_i - y_0 \\ \hat{r}_i &= \sqrt{\hat{x}_i^2 + \hat{y}_i^2} \\ \hat{\theta}_i &= \tan^{-1}\left(\frac{\hat{y}_i}{\hat{x}_i}\right) \end{aligned}$$

Fourier transform

We expand using a discrete Fourier transform,

$$\begin{aligned} \hat{a}_j &= \frac{1}{\pi}\sum_{k=1}^{M}\left[\hat{r}_k \cos\left(j\hat{\theta}_k\right)\Delta\hat{\theta}_k\right] \\ \hat{b}_j &= \frac{1}{\pi}\sum_{k=1}^{M}\left[\hat{r}_k \sin\left(j\hat{\theta}_k\right)\Delta\hat{\theta}_k\right] \end{aligned}$$

where M is the number of samples taken in each turn (360 on average).

Shape reconstruction

$$\hat{r}(\theta) = R_0 + \sum_{j=1}^{N} \left[\hat{a}_j \cos(j\theta) + \hat{b}_j \sin(j\theta)\right]$$

where N is the number of modes used in the reconstruction of the shape.

Sampling theorems [7] put a limit on the maximum value of N that can be used (in our case $N < (M/2) \simeq 180$, typically 50). For practical purposes we define the amplitude of the j mode of the Fourier decomposition as,

$$A_j = \sqrt{\hat{a}_j^2 + \hat{b}_j^2}.$$

A.3 Mapping of the Sample Wall Thickness

A regular mesh is drawn on the samples external surface (see Fig. A.1) and at the mesh nodes the thickness is measured using standard manual ultrasonic gages.

A.4 Deepwater Pipelines: Measurements

The scope of this Section is to describe the results of the geometrical survey of the 9 samples of the tests described in Chap. 4. The geometrical survey is composed by the mapping of the external surface and the measurement of the wall thicknesses.

The results of the topography mapping of the external surface, the modal analysis of the circular deviations and the wall thickness are analyzed. The samples belong to two different mills.

Table A.1 summarizes the main characteristics of the samples.

Pipe Survey

Fourier analysis of the circular deviations

Figure A.3 shows, for samples 1–3, the Fourier series decomposition of the deviations with respect to the average diameter.

Table A.1 Samples description

Sample	Nominal OD [mm]	Nominal thickness [mm]
1	353.00	22
2	353.00	22
3	353.00	22
4	323.85	17.65
5	323.85	17.65
6	323.85	17.65
7	323.85	20.30
8	323.85	20.30
9	323.85	20.30

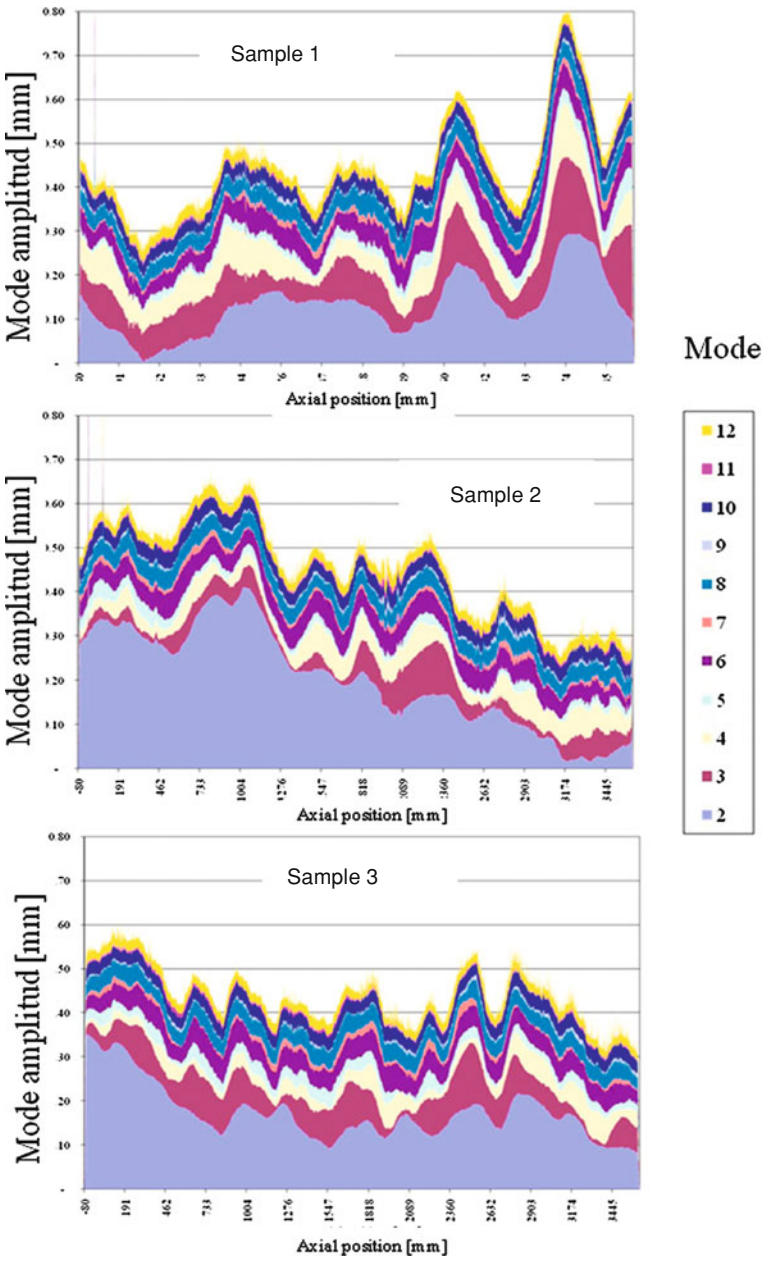

Fig. A.3 Samples 1–3: modal analysis: mode amplitude distribution along the sample

The specimens are 4 m long. The grid has 48 longitudinal sections with a 75 mm spacing, and 16 circumferential generatrices, giving 768 grid points.

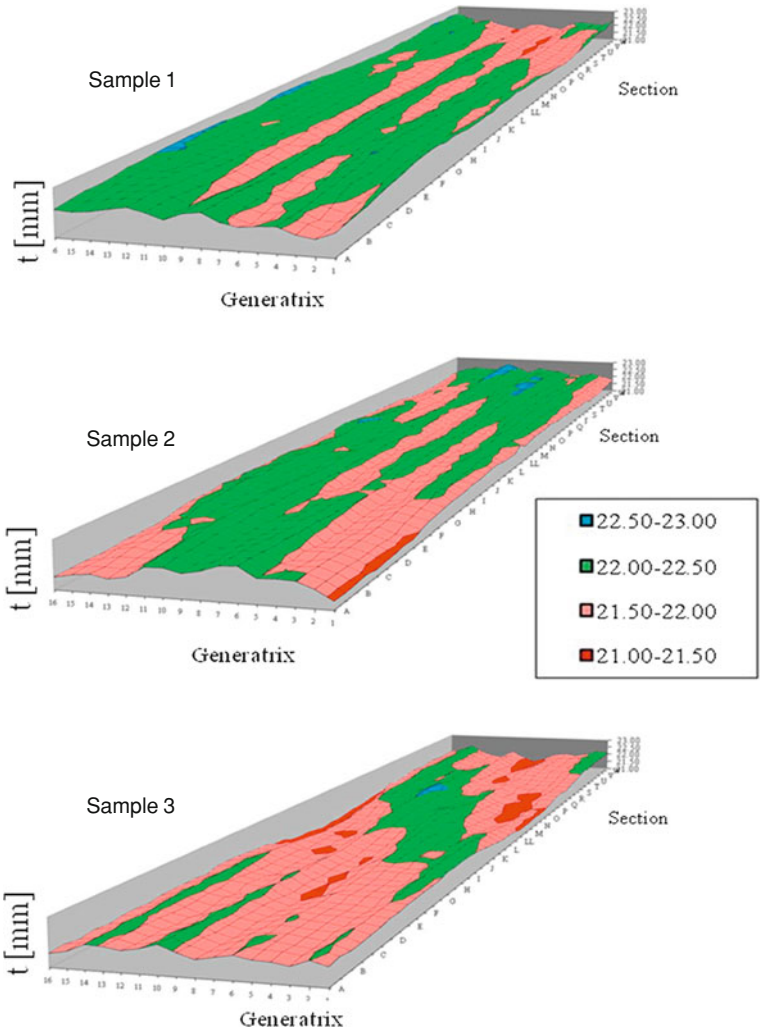

Fig. A.4 Samples 1–3, wall thickness distribution

In Fig. A.4 we show a representation of the thickness distribution for the first three samples.

A.5 Deepwater Pipelines with Buckle Arrestors: Measurements

For a sample made of two pipes with a welded intermediate arrestor the outside surface Fourier decomposition is shown in Fig. A.5 and the thickness distribution of the two pipes in Fig. A.6.

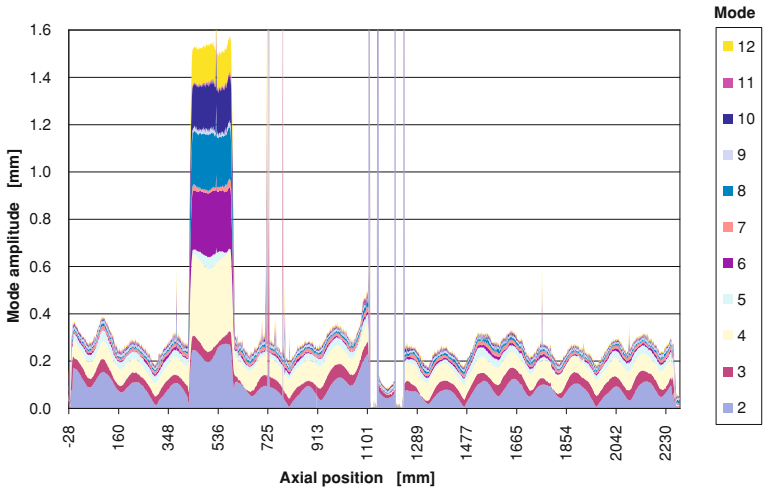

Fig. A.5 Outside surface Fourier decomposition of sample #1

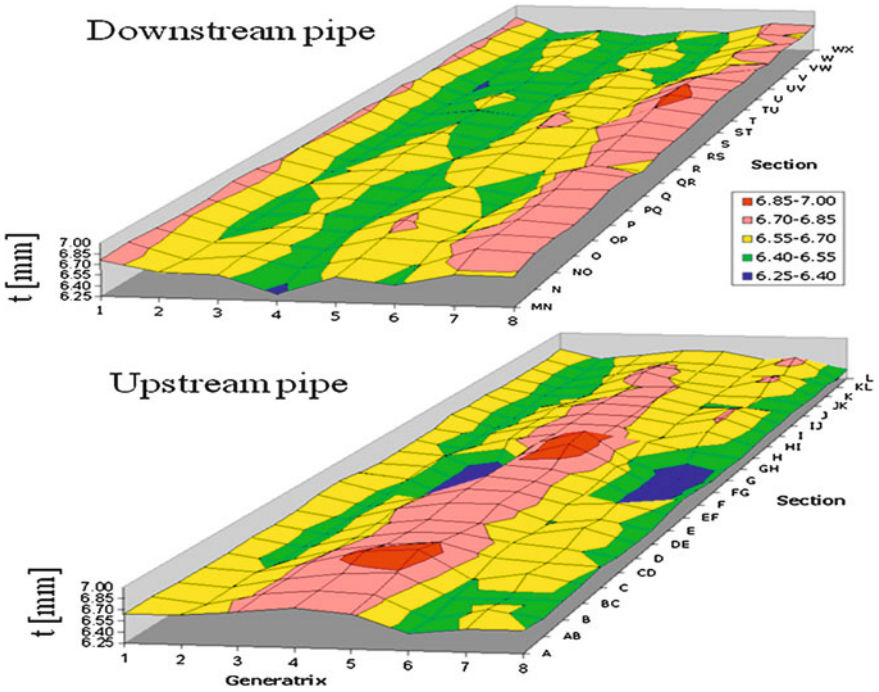

Fig. A.6 Sample #1–5 9/16″ OD 6.55 mm WT AST A-333. Thickness distribution

References

1. Arbocz J, Babcock CD (1969) The effect of general imperfections on the buckling of cylindrical shell. ASME J Appl Mech 36:28–38
2. Arbocz J, Williams JG (1977) Imperfection surveys of a 10-ft diameter shell structure. AIAA J 15:949–956
3. Yeh MK, Kyriakides S (1988) Collapse of deepwater pipelines. ASME J Energy Res Technol 110:1–11
4. Assanelli AP, Toscano RG, Johnson D, Dvorkin EN (2001) Experimental/numerical analysis of the collapse behavior of steel pipes. Eng Comput 17:459–486
5. Press WH, Flannery BP, Teukolsky SA, Veherling WT (1986) Numerical recipes. Cambridge University Press, Cambridge
6. Shunmugam MS (1991) Criteria for computer-aided form evaluation. ASME J Eng Ind 113:233–238
7. Brigham EO (1988) The fast Fourier transform and its applications. Prentice Hall, New Jersey